Applied Catalysis B: Environmental 160–161 (2014) 456–464

Contents lists available at ScienceDirect

Applied Catalysis B: Environmental

journal homepage: www.elsevier.com/locate/apcatb

Nanoneedle and nanotubular titanium dioxide – PES mixed matrix membrane for photocatalysis

Kristina Fischer[a], Roger Gläser[b], Agnes Schulze[a,*]

[a] Leibniz Institute of Surface Modification, Permoserstraße 15, Leipzig D-04318, Germany
[b] Leipzig University, Institute of Chemical Technology, Linnéstraße 3, Leipzig D-04103, Germany

ARTICLE INFO

Article history:
Received 21 March 2014
Received in revised form 28 May 2014
Accepted 31 May 2014
Available online 6 June 2014

Keywords:
TiO_2 nanotubes
Photocatalysts
PES membranes
Thin films

ABSTRACT

A method to synthesize TiO_2 nanotubes via anodization on a porous polymer material, namely a polyethersulfone membrane, is reported. The TiO_2 nanotubes can be easily designed by sputtering a titanium film on top of the membrane, followed by anodization of titanium to TiO_2 nanotubes. Subsequent crystallization to photocatalytically active anatase nanoneedle and nanotubular structures is performed under mild conditions at temperatures below 120 °C, thus enabling the use of a polymer substrate. The hybrid system is mechanically stable and flexible at all stages of the assembling process. Because of the enhanced surface area and light-harvesting capability of the anatase nanoneedle and nanotubular structures on the membrane a high photocatalytic activity is achieved. This method will reasonably expand the application of TiO_2 nanotubes for different substrates and open up new catalytic setups and novel products.

1. Introduction

Since Zwilling [1,2] and co-workers discovered the formation of nanotube-like TiO_2 through anodization of titanium in chromic acid and hydrofluoric acid in 1999, there has been an increasing interest in the synthesis of TiO_2 nanotubes via anodization. TiO_2 is a non-toxic, environmentally friendly, and corrosion-resistant material with a high photocatalytic activity and photoelectric conversion efficiency [3]. The surface-area-to-volume ratio of TiO_2 nanotubes is increased enormously compared to 2D structures. Furthermore, the electron transport velocity and charge separation efficiency is increased due to the nanotubular structure, and charge recombination at interfaces is reduced, making it an ideal material for solar energy conversion applications [4–7]. The photocatalytic reactions of TiO_2 do only work with light in the UVA-region due to the large band gap of TiO_2. Therefore the narrowing of the band gap, i.e. changing the photoresponse from UV to visible light is desirable and can be done by doping the nanotubes with suitable atoms [8,9].

Using the biocompatible properties and good cell adhesion performance, TiO_2 nanotubes are also suitable as implantation materials [10–13]. Based on the large surface and semiconducting quality of TiO_2, the nanotubes can work as gas-sensors as well [14–16]. TiO_2 nanotubes can also operate as membranes [17,18], as electrodes [19,20] and are able to split water into H_2 and O_2 [7,21]. On the basis of the above mentioned photocatalytic properties TiO_2 nanotubes that are immobilized on a support remove organic contaminations from water and air [18,22–29] and do not have to be separated from a slurry system after photocatalytic reaction as it would be the case when using TiO_2 in form of a powder.

The length of TiO_2 nanotubes is limited by the chemical dissolution of TiO_2 at the tube opening, which is induced by fluoride ions in acidic solutions. Therefore the first nanotubes anodized in highly dissolving aqueous acidic HF-containing electrolyte yield only lengths up to 500 nm [30]. Through tuning the pH of KF and NaF aqueous electrolytes, the chemical dissolution is reduced and nanotubes up to a length of several microns were achieved [31]. By changing the electrolyte solution from water-based to organic liquid-based such as ethylene glycol, di-ethylene glycol, formamide, *N*-methylformamide and dimethyl sulfoxide in combination with HF, KF, NaF, NH_4F, Bu_4F or $BNMe_3NF$ a huge increase in length is generated [31–36]. Paulose et al. even established nanotubes with a length of 1000 μm by anodizing 1.0 mm thick Ti sheet at 60 V for 9 days in ethylene glycol [37]. Allam et al. were able to synthesize TiO_2 nanotubes in fluorine free electrolytes using HCl instead [38,39] reaching lengths up to 900 nm [38].

Despite the large number of publications on TiO_2 nanotubes, minor attention has been addressed to alternative carrier materials other than titanium [6,32,39–50], especially to polymer substrates [6,40,41,49]. The combination of TiO_2 nanotubes with a polymer

* Corresponding author. Tel.: +49 3412352400.
E-mail addresses: kristina.fischer@iom-leipzig.de (K. Fischer), roger.glaeser@uni-leipzig.de (R. Gläser), agnes.schulze@iom-leipzig.de (A. Schulze).

http://dx.doi.org/10.1016/j.apcatb.2014.05.054
0926-3373/

can offer new properties and applications. The preparation of many polymers is fast and inexpensive, and many different shapes and properties are accessible. The TiO_2 nanotubes on top of the polymer are mechanically stable and can be handled easily in contrast to a freestanding TiO_2 nanotube membrane [17,51,52]. To the best of our knowledge, there is only one publication regarding TiO_2 nanotubes established on a rough substrate (aluminum) [25,40] and not one on a porous substrate. By attaching TiO_2 in form of nanotubes on a porous substrate, the overall active surface area shall be increased. Therefore, surface-sensitive reactions will be enhanced, e.g. photocatalytic degradation of environmental pollutants or solar cell efficiency due to a higher dye adsorption [53]. By using porous substrates various media (gas or liquid) can be soaked or purged through the substrate. Excellent contact properties will arise, e.g. in photocatalytic reactions, the molecule to be degraded is transported right to the reaction location.

Here we show for the first time the synthesis of TiO_2 nanotubes on top of a porous polyethersulfone (PES) polymer membrane (see Fig. 2). We used a nonaqueous electrolyte (ethylene glycol) containing ammonium fluoride to avoid the usage of highly toxic hydrofluoric acid. The TiO_2 nanotubes were well attached to the membrane. The membrane could be bent to a large scale without destroying or separating the nanotubes from the membrane and even touching the surface did not cause any detachment. The TiO_2 nanotubes were crystallized to photocatalytically active anatase with water in its liquid (hydrothermal) and vapor (vapor-thermal) form at temperatures below 120 °C to nanoneedle and nanotubular structures, respectively. The crystallization with water promotes the adsorption of OH species on the surface of TiO_2 and therefore increases the photocatalytic degradation of dyes [25,54]. The TiO_2 nanotube arrays after hydrothermal crystallization even have a higher photocatalytic rate constant compared to P25 nanoparticles as shown by Krengvirat et al. [54]. Vapor-thermal and hydrothermal crystallized TiO_2 nanotubes on the membrane had the same photocatalytic degradation activity of methylene blue and up to 5–6 times higher compared to a smooth TiO_2 film on the membrane. The assembly of TiO_2 nanotubes on a porous membrane led to an again increased photocatalytic activity compared to TiO_2 nanotubes on a Ti foil as the membrane support provided another gain in surface area.

2. Experimental

2.1. Materials

Ethylene glycol (≥99%, for synthesis) was purchased from Carl Roth GmbH+Co. KG. Ammonium fluoride (for analysis EMSURE® ACS) was obtained from Merck KGaA. Palladium foil (99.9%, 1 mm thick), palladium wire (99.9%, 1.0 mm diameter) and titanium foil (99.6%, 0.05 mm thick) were purchased from ChemPur Feinchemikalien und Forschungsbedarf GmbH. Deionized water was obtained from *Milli-Q water* filtration station (Millipore). Polyethersulfone membrane (Millipore Express® PLUS Membrane Filters, HPWP14250, pore size 0.45 μm) was purchased from Merck Millipore. Methylene blue was obtained from Acros Organics (96+%, high purity).

2.2. Coating with titanium

A titanium film was magnetron-sputtered onto polyethersulfone membrane to a thickness of 900 nm and onto silicon wafer to a thickness of 800 nm with a Leybold Z 400. The sample was mounted to a sample holder at a distance of 47 mm to the target. The pressure in the chamber was set to 8×10^{-3} bar. The sample holder was cooled with water during sputtering. The sputtering atmosphere was argon and the sputtering power density was set to 150 W.

2.3. Synthesis of TiO_2 nanotubes

Before anodization of the titanium-coated membrane, wafer or Ti foil, the electrolyte was aged by anodizing a titanium foil for several hours. This aged electrolyte can be used for several anodizations and gives clean and strongly attached nanotubes [55]. The titanium-coated support (membrane, wafer or Ti foil) was anodized by placing it in a two-electrode configuration, in which the support operates as the working electrode and the palladium foil as the counter electrode. The potential was kept constant at 40 V. The anodization was observed by monitoring the current during the anodization with a multimeter (Rigol Digital Multimeter 3051). The support was kept in the electrolyte solution after termination of the anodization for up to 30 min in order to prevent surface aggregation [55]. The electrolyte solution was prepared from ethylene glycol containing ammonium fluoride (1.2 wt% or 1.4 wt%) and deionized water (2 vol%). The anodized support was rinsed with deionized water and washed twice for 15 min with deionized water before drying in air.

2.4. Crystallization to anatase

TiO_2 was crystallized with water at low temperatures or calcined at high temperatures in air. The water crystallization works either with liquid water (hydrothermal) or vapor water (vapor-thermal). Amorphous TiO_2 was treated in 200 mL deionized water at 90 °C up to 2 h (hydrothermal) or in a Teflon flask at 110 °C with 50 μL of deionized water for up to 1 h (vapor-thermal). For the vapor-thermal method the water was added to a small glass beaker inside the Teflon flask to avoid contact of the TiO_2 with liquid water. The Teflon flask was closed, placed in a high pressure protective shell (DM00059, MWS GmbH) and sealed in a rotor segment (HPR-1000/10S with APCU-100, MWS GmbH).

The calcination of TiO_2 nanotubes on the silicon wafer was done by placing the substrate in an Al_2O_3 crucible which then was transferred to an oven (HT 08/17l, Nabertherm). The oven was heated at a rate of 3 K/min to 450 °C. After 5 h at 450 °C the oven was cooled to room temperature at a rate of 3 K/min [25,45,56].

2.5. Characterization

The morphology of the TiO_2 nanotubes was characterized using a field emission scanning electron microscope (FESEM; Zeiss Ultra 55). The X-ray diffraction (XRD) was always measured with TiO_2 nanotubes assembled on Si wafers as otherwise the amorphous PES peak of the membrane did dominate the results. The XRD patterns were observed on an Ultima IV X-ray diffraction spectrometer (Rigaku) with Cu Kα radiation and operated at 40 kV and 40 mA with a scanning speed of $1^\circ\,\mathrm{min}^{-1}$ at a step size of 0.01°. The crystallite sizes of TiO_2 were determined by using Scherrer's equation ($d = 0.9\lambda/B\cos\theta$), where d, λ, B, and θ are crystallite size, Cu Kα wavelength (0.15418 nm), full width at half–maximum intensity (fwhm) of the (1 0 1) reflection of anatase in radians, and Bragg's diffraction angle, respectively [57]. X-ray photoelectron spectroscopy (XPS) was performed on Axis Ultra (Kratos Analytical Ltd., Manchester; UK) with monochromatic Al Kα cathode, an X-ray source with 150 W power and 40 eV pass energy. Light absorption properties were measured with UV–vis diffuse reflectance spectrometer (Cary 5000, Agilent, USA), and spectralon was used as a reflectance standard. The photoactivity of the TiO_2 nanotubes and film on the PES membrane and the TiO_2 nanotubes on the Ti foil were tested by degradation of methylene blue [58–60] in aqueous solution at room temperature. The samples (cut to circles with

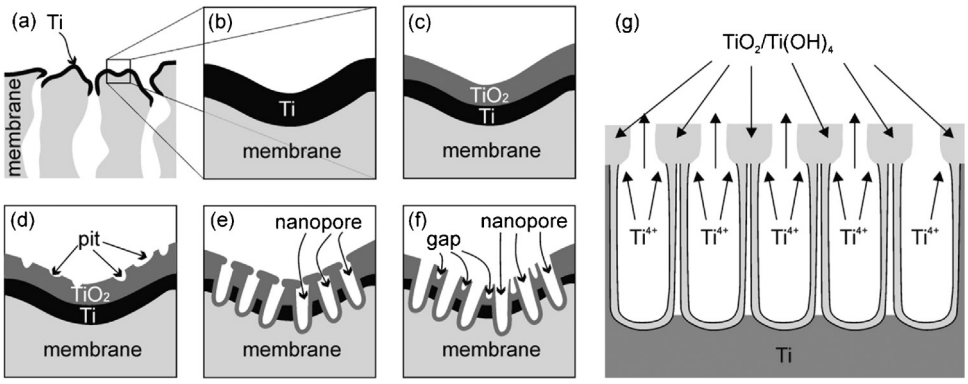

Fig. 1. A schematic diagram of the growth mechanism of TiO_2 nanotubes on a membrane is displayed. (a) Membrane with titanium film on the surface, (b) enlarged viewing of the titanium coated surface of (a), (c) a compact layer of TiO_2 does grow via anodization of titanium, (d) F^- etches unregularly pits into TiO_2, (e) progressive etching leads to ordered nanopores with $Ti(OH)_4$ precipitates at the opening, (f) formation of open nanopores with gaps with consecutive anodization/etching (g) generation of $TiO_2/Ti(OH)_4$ at the pore opening with unfavorable conditions.

$d = 2.5$ cm and a circular hole in the middle with $d = 1$ cm for spectrometric measurement) were placed in a 6-well plate (Thermo Fisher Scientific, Nunclon Delta Surface), and 4 mL of a 20 μmol L^{-1} methylene blue solution was added. The plate was placed below a UVA-lamp (Heraeus Original Hanau Suncare tanning tube OH N 21/25 Slim, radiant flux density 7.6 mW cm^{-2}) and was shaken on a Titramax 100 (Heidolph Instruments GmbH & Co. KG) with 200 rpm during radiation. The degradation of methylene blue was measured by putting the plate into the spectrometer (Tecan Reader infinite M200) and measuring the absorption at 660 nm periodically. The rate constant was evaluated via a first order kinetic. The slope of logarithmic c/c_0 over time is the rate constant.

3. Results and discussion

3.1. Nanotube preparation

To fabricate the TiO_2 nanotube PES membrane system a layer of titanium is sputtered onto the PES membrane before anodization can take place to form nanotubes (see Section 2.2 for details). The sputtering process of the titanium film on the membrane needs to meet certain criteria. First, the generated heat must be removed to avoid destruction of the membrane. Therefore the sputtering time, i.e. the film thickness is limited to 400 nm. To generate thicker films the sputtering was repeated for a couple of times. Secondly, blocking of the membrane pores by the sputtered titanium film and further on by the TiO_2 nanotube array must be obviated. And thirdly a thick layer of titanium makes the substrate more brittle and less elastic.

For the generation of TiO_2 nanotubes a thick layer of titanium is needed. The reasons are discussed below. Taking all these factors into account, we were able to achieve a 900 nm (repeated sputtering for 3 times of 300 nm) thick layer of titanium on the membrane. A membrane with a pore size of 0.45 μm was chosen to avoid blocking of the pores. When using a membrane with a pore size of 0.22 μm and below, the pores were blocked by the TiO_2 nanotube array. With a layer of 900 nm titanium the pores of the membrane are still open and the membrane properties are not altered (e.g. water permeability).

The mechanism of TiO_2 nanotube assembly on a membrane is shown in Fig. 1. With the start of the anodization an oxide film barrier layer is generated on the surface of the titanium film. F^- attacks the TiO_2 barrier layer under the influence of the electric field at the anode to form TiF_6^{2-}, which is soluble in the electrolyte (υ_{dis}). Small pits are generated unregularly over the whole surface. At the same time Ti is electrochemical dissolved and Ti^{4+} is ejected from the nanopores to the outside and accumulate as TiO_2 or $Ti(OH)_4$ via hydrolysis reaction ($\upsilon_{electro}$, Fig. 1e and g) [61]. In the beginning the electrochemical dissolution ($\upsilon_{electro}$) dominates the process as the oxide barrier is thin and a high electrical field is conserved. With consecutive formation and etching of TiO_2 the process leads to ordered nanopores because the chemical etching (υ_{dis}) is preferred. As the oxide film thickness between the pores is becoming relatively thicker, the electrochemical corrosion is concentrated in dissolving TiO_2 at this site and forming small gaps between the pores. A uniformly distributed film of nanotubes on the membrane surface is formed. With a thin titanium film (below 2 μm) the anodization had to be stopped at an early stage (<10 min) so that $\upsilon_{dis} < \upsilon_{electro}$. The pores are blocked by surface debris consisting of $Ti(OH)_4$ or/and TiO_2 (Fig. 1e and g) [61]. The chemical dissolution (υ_{dis}) needs to be increased. By changing the composition of the electrolyte solution, the voltage, temperature, and other factors the ratio could be changed to form unblocked nanotubes at an early stage of the TiO_2 nanotube formation [50,61].

Table 1
Increasing the voltage of the anodization leads to magnified tube diameter. To gain unblocked nanotubes the amount of NH_4F had to be increased.

Voltage (V)	Amount of NH_4F (wt%)	Tube diameter (nm)
15	0.8	13–15
20	1.2	27–30
30	1.2	32–35
40	1.4	38–42

With a thickness of 900 nm, an electrolyte solution containing 3 vol.% water and 0.8 wt% ammoniumfluoride in ethylene glycol, a voltage of 15 V and an anodization at room temperature clean and freestanding nanotubes on a membrane were achieved (Fig. 2, for specification see supplementary information). The TiO_2 nanotubes were well attached to the membrane and did adopt the flexibility and stability of the membrane (Fig. 3). In contrast to self-supported TiO_2 nanotubes, which are very brittle and fragile [52], the TiO_2 nanotube supported membrane can be bent at a large scale.

By increasing the voltage of the anodization the tube diameter can be increased [3]. Starting at 13 nm with a voltage of 15 V the tube diameter was raised up to 42 nm with a voltage of 40 V (Table 1). Nanotubes generated at a higher voltage than 40 V were not achieved due to the emerging high current (high temperature) in combination with such a thin titanium film on a PES membrane support. When increasing the voltage of the anodization the amount of ammonium fluoride had to be increased to avoid the formation of again generated surface debris.

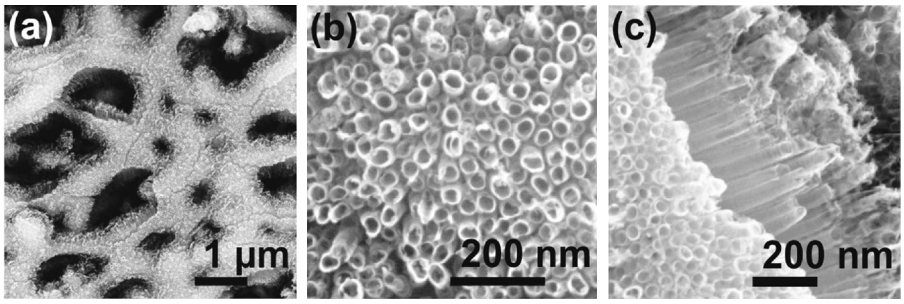

Fig. 2. FESEM images of as-anodized TiO_2 nanotube arrays on top of a PES membrane: top view (a and b); and cross-sectional view (c).

3.2. Crystallization at low temperature

In order to use the photocatalytic properties of TiO_2, the as-anodized TiO_2 nanotubes, which are amorphous and non-photoactive, need to be crystallized to the most photoactive phase, i.e. anatase [56]. Calcination of TiO_2 nanotubes at temperatures above 400 °C is not possible due to the low glass transition temperature (204 °C) of the support membrane material PES [62]. By using water as a transformation catalyst, the crystallization temperature can be lowered to room temperature [25,54,57,63,64]. The surface area compared to as-anodized and calcined nanotubes is also increased by about 5.5 [63] and 4.2 times, respectively due to crystallization with water [54]. Water was used in form of its steam at 110 °C (vapor-thermal) and in liquid form at 90 °C (hydrothermal). These relatively high temperatures were chosen to enhance the crystallization process.

The evolving reflection in the X-ray diffractogram (Fig. 4) corresponds to the (1 0 1) diffraction plane of anatase TiO_2 (JCPDS No. 21-1272, a = 3.7852 Å, c = 4.683 Å, space group: $I4_1/amd$ (1 4 1)). The peak of the calcined nanotubes is smaller compared to the anatase peak of the hydrothermal and vapor-thermal crystallized nanotubes. This is also reflected by the relative crystallinity factor (the relative intensity of the diffraction peak from the anatase (1 0 1) plane compared to calcined TiO_2 nanotubes) of the vapor-thermal and hydrothermal crystallized samples, which were 7.61 and 5.24, respectively (Table 2). This indicates a high catalytic effect of water for crystallizing amorphous TiO_2 to anatase TiO_2 at low temperatures [25]. In addition the crystallized TiO_2 with water has a higher degree of OH species at its surface which increases the photocatalytic degradation of dyes [25,54].

The crystallization by the vapor-thermal method depended strongly on the amount of water added to the system (Fig. 5). With increasing volume of water, the crystallite size and relative crystallinity did increase until a plateau was reached (Fig. 5 and Table 2). Starting at a volume of 30 µL (time and temperature is set at 120 min and 110 °C, respectively) the diameter of the anatase crystals were 3.18 nm and a relative crystallinity of 2.18 was achieved. When doubling the volume to 60 µL the crystallite size was about

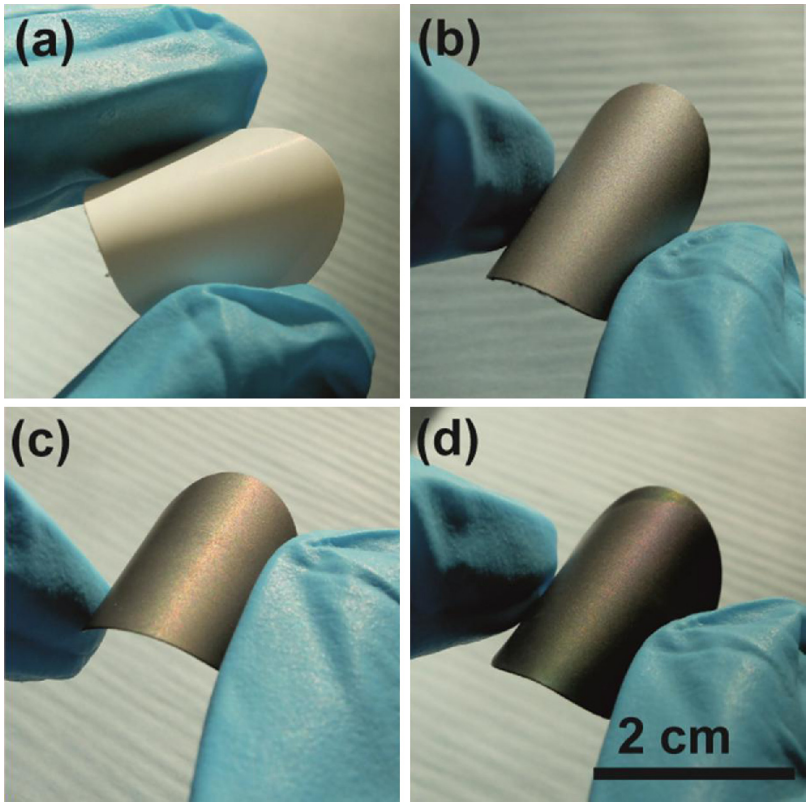

Fig. 3. Photographic images of the membranes showing its flexible properties at each stage of the preparation process. (a) PES membrane, (b) PES membrane with titanium on top, (c) PES membrane with TiO_2 nanotube arrays on top, (d) PES membrane with crystallized TiO_2 nanotubes on top.

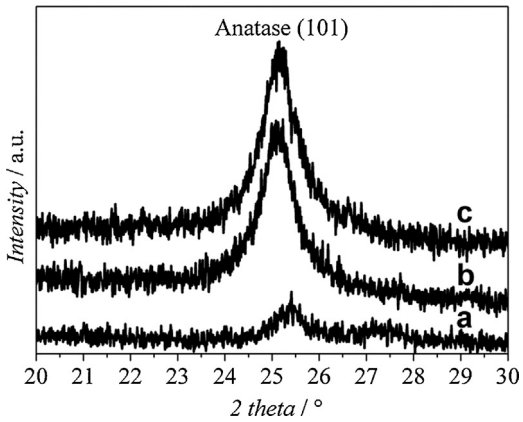

Fig. 4. XRD patterns of crystallized TiO_2 nanotubes on top of a Si wafer. (a) Calcined nanotubes at 450 °C for 5 h, (b) vapor-thermal crystallized nanotubes at 110 °C with 50 μL of water for 1 h and (c) hydrothermal crystallized nanotubes at 90 °C for 2 h.

Table 2
Crystallite size calculated by Scherrer's equation and relative anatase crystallinity.

Treatment methods	T (°C)	t (min)	V (μL)[a]	d (nm)[b]	RC[c]
As-anodized				0	0
Calcination	450	300		11.52	1
	110	30	50	8.80	5.18
	110	60	50	9.21	4.81
Vapor-thermal	110	120	50	12.71	7.41
	110	120	30	3.18	2.18
	110	120	40	9.69	2.18
	110	120	60	12.86	7.61
	90	30		0	0
Hydrothermal	90	60		9.47	2.38
	90	120		8.80	5.24

[a] Volume of added water to the Teflon flask for the vapor-thermal crystallization.
[b] Crystallite size.
[c] Relative crystallinity: the relative intensity of the diffraction peak from the anatase (1 0 1) plane (reference = calcined TiO_2 nanotubes).

4 times higher (12.86 nm) and the relative crystallinity increased up to 7.61.

The crystallite size and relative crystallinity also increased with longer crystallization time for both crystallization methods (Fig. 6 and Table 2) until a constant value was reached. After 30 min of crystallization via the vapor-thermal method (110 °C, 50 μL) anatase crystals with a diameter of 8.80 nm and a relative crystallinity of 5.18 were obtained. Crystallization of the TiO_2 nanotubes with hydrothermal crystallization was slower, after 30 min at 90 °C no anatase crystals were observed. Increasing the crystallization time to 120 min crystals with a diameter of 12.71 nm

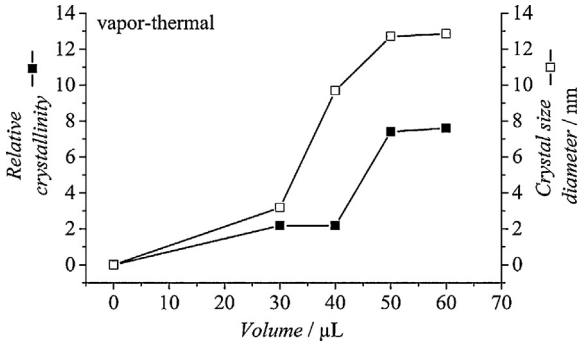

Fig. 5. Relative crystallinity and crystal size of vapor-thermal crystallized nanotubes as a function of added volume of water.

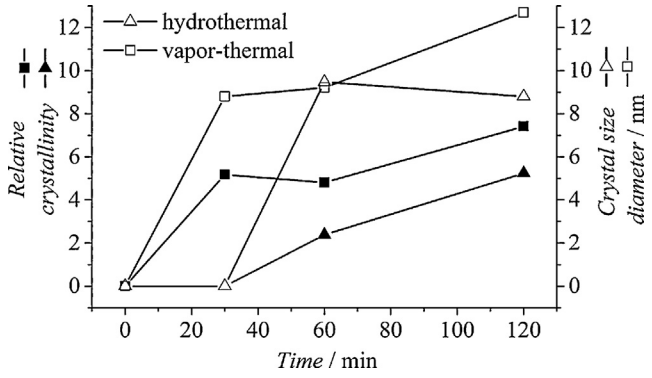

Fig. 6. Relative crystallinity and crystal size of hydrothermal (△,▲) and vapor-thermal (□,■) crystallized nanotubes as a function of time.

for vapor-thermal crystallization and crystals with a diameter of 8.80 nm for the hydrothermal method were obtained. The relative crystallinity after 120 min for vapor-thermal and hydrothermal crystallization was set at 7.41 and 5.24, respectively. The higher crystallization temperature for the vapor-thermal crystallization of 110 °C compared to 90 °C for hydrothermal crystallization leaded to an acceleration of crystal growth.

While the nanotube morphology persisted upon vapor-thermal treatment, the crystallization by the hydrothermal method totally transformed the nanotubes to a nanoneedle-like structure (see Fig. 7) [25,54,63–65]. An amorphous TiO_2 film (smooth) on top of the membrane (Ti film with thin layer of TiO_2 oxidized in air at room temperature) was also crystallized by the vapor-thermal method to compare it with the TiO_2 nanotubes (Supplementary information Fig. S3). A change in morphology as it was the case for TiO_2 nanotubes of the crystallized TiO_2 film is not visible, because the film was not structured (smooth) before crystallization.

Also TiO_2 nanotubes on thin Ti foil were prepared and crystallized via vapor-thermal method. The photocatalytic activity of a smooth anatase TiO_2 film on a membrane, with a porous anatase TiO_2 morphology (nanotubular and nanoneedle like structures) on a membrane and Ti foil were compared (see Section 3.4).

3.3. Chemical and optical characterization

To investigate surface composition and chemical status of TiO_2 nanotubes before and after crystallization XPS measurements (Fig. 8) were carried out. The survey spectra in Fig. 8I show that titanium, oxygen, fluorine, nitrogen and carbon existed on the surface of untreated and crystallized TiO_2 nanotubes. Carbon is principally monitored in XPS spectra occurring from different kind of sources, e.g. from the XPS instrument itself or from the environment as hydrocarbons [25,46,54]. Part of the carbon signal here can be attributed to adsorbed electrolyte (ethylene glycol), although the sample was washed twice with water for 15 min. The small value of nitrogen (1.1–2.0%) on the surface can be attributed to adsorbed NH_4^- residuals from the NH_4F in the electrolyte. The high resolution spectra of O1s in Fig. 8II can be fitted by three Gaussian components at 530.4, 532.0 and 533.7 eV. The peak at 530.4 eV is attributed to Ti—O in TiO_2, while the peak at 532.0 eV is assigned to surface hydroxyl groups O—H. The third small peak at 533.7 eV is ascribed to adsorbed O_2 [66]. The ratio of the Ti—O peak to the O—H peak is changing with crystallization of the TiO_2 nanotubes. The untreated TiO_2 nanotubes exhibited a high amount of O—H groups on the surface coming from Ti—OH and residual ethylene glycol. With crystallization, especially hydrothermal crystallization, the amount of O—H groups on the surface decreased. This can be explained by two factors. One is that the alcohol groups

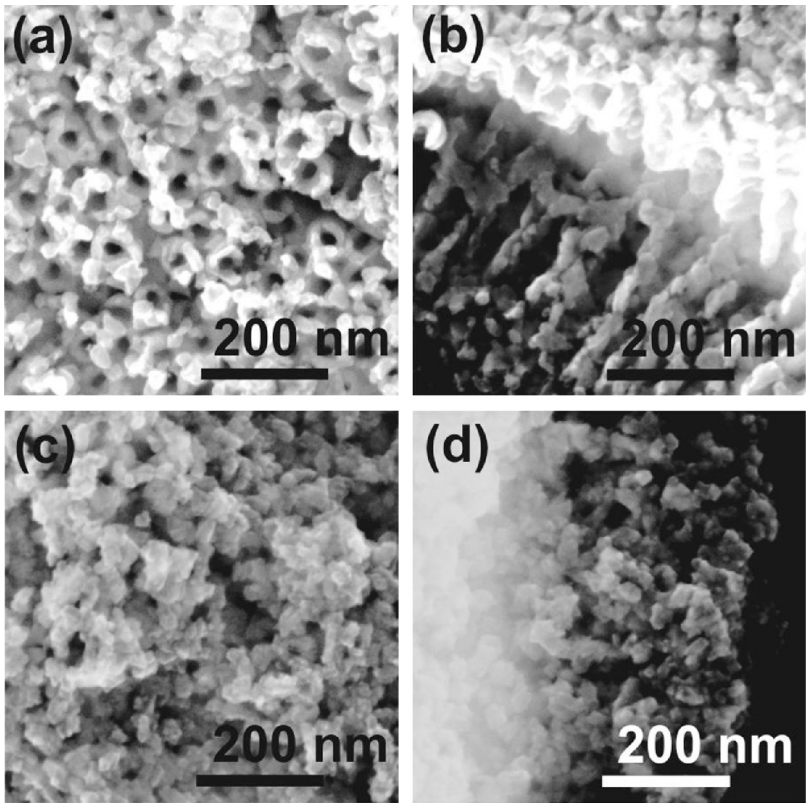

Fig. 7. FESEM images of crystallized TiO_2 nanotube array on top of a PES membrane. Nanotubular TiO_2 arrays through vapor-thermal crystallization: (a) top view, (b) cross-sectional view. Nanoneedle TiO_2 array through hydrothermal crystallization: (c) top view; (d) cross sectional view.

(C—O—H) related to ethylene glycol was removed from the surface via the crystallization process. In the case of hydrothermal crystallization water was used as a dissolution agent leading to a smaller O—H peak compared to vapor-thermal crystallization as it can be seen in Fig. 8II(b).

Another factor related to the reduction of O—H groups can be the dehydration reaction (Ti—OH + Ti—OH → TiO_2 + H_2O) on the surface [25]. The high resolution spectra of F1s at 684.9 eV (Fig. 8III) show also a decrease of the element fluorine with crystallization. The F1s peak belongs to surface fluoride (Ti—F) formed by ligand exchange between fluoride and surface hydroxyl groups [25]. Untreated TiO_2 nanotubes contained the highest amount of the element fluorine due to its amorphous structure and surface fluorination. Via hydrothermal treatment absorbed fluoride was dissolved in water.

The light absorption of amorphous and anatase TiO_2 nanotubes on the membrane in the UV–vis range was obtained by UV–vis diffuse reflectance spectroscopy. The amorphous TiO_2 nanotubes exhibit an absorption band of about 400 nm (Fig. 9). The absorption characteristics of amorphous TiO_2 are quite similar to anatase TiO_2 as discussed in the literature [67,68] and obtained here (Fig. 9). The absorption band of the anatase TiO_2 nanotube on the membrane can be divided into two parts. Starting at about 320 nm the absorption dropped (shoulder band) until 370 nm were a tail-like band continued to a wavelength of about 500 nm. According to Krengvirat et al. this absorption band evolution fits quite well to that of carbon-doped TiO_2 [54]. The electronic transition from O2p to Ti3d orbitals is primarily responsible for the absorption of light. When carbon is inserted into TiO_2 a C2p state is generated, which lowers the E_B and generates the split into a shoulder band and tail-like band [54]. A small redshift of about 10 nm was obtained for the vapor-thermal crystallized TiO_2 nanotubes. Additionally according to Peralta-Hernandez et al. [69] interstitial carbon can prevent the recombination of charge carriers, thus increasing the photocatalytic activity of the system.

3.4. Photocatalytic activity

To enable an easy comparison with other systems reported in the literature, we decided to demonstrate the photocatalytic activity of our hybrid system using methylene blue as a model system.

The nanostructured TiO_2 on the membranes showed a high photocatalytic activity in degrading methylene blue after crystallization, as expected. The structure and porosity of the TiO_2 system has a drastic impact on the rate constant, because a porous and structured material has a higher surface area and thus more reaction spots. The rate constant was increased by a factor of 5–6 with the nanotubular/nanoneedle-like TiO_2 structured film on the membrane when compared to a smooth TiO_2 film on the membrane (Fig. 10b). The membrane as the support material has also an impact on the photocatalytic activity compared to a Ti foil (Fig. 10) due to the porous surface of the membrane, thus the rate constant was again increased.

The photocatalytic degradation of many different molecules (i.e. dyes, drugs or pesticides) with TiO_2 has been thoroughly discussed in the literature [70–77]. TiO_2 generates an electron-hole pair via the absorption of UVA-light. The excited electrons react with O_2 to generate a superoxide radical ion O^{2-} while the holes do react with water to form highly reactive hydroxyl radicals •OH. The hydroxyl radicals are the major active species for the photocatalytic degradation of organic molecules. A high amount of •OH is therefore preferable and is achieved by crystallization of amorphous TiO_2 to anatase [78]. Rutile TiO_2 has a lower amount of •OH at its surface. Methylene blue is photocatalytically degraded via several intermediates to form inorganic products and carbon dioxide. According to the literature [58] the cleavage of the C—S^+=C group is initiated

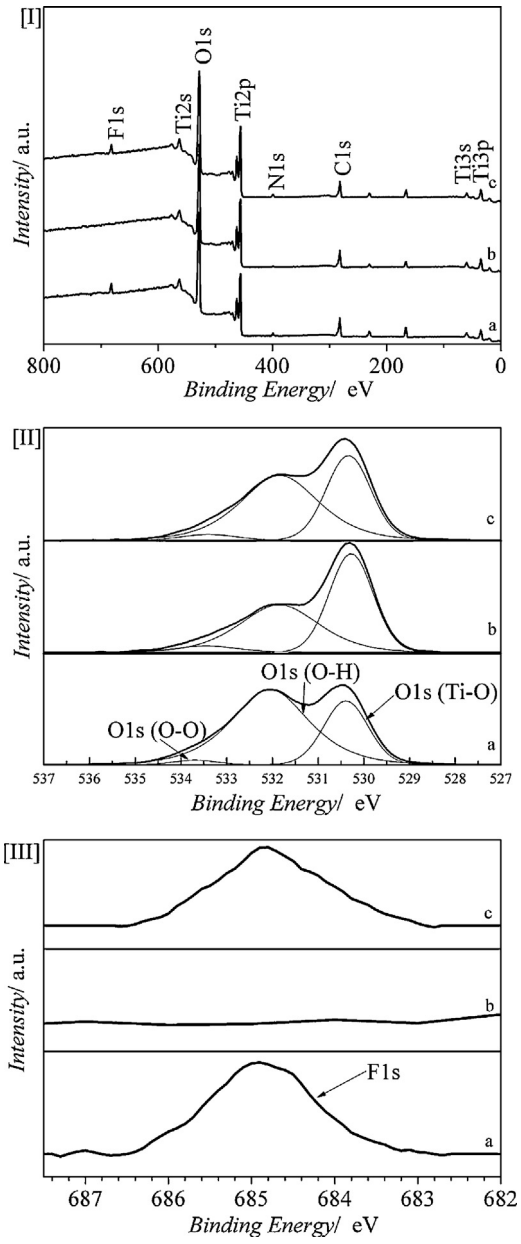

Fig. 8. XPS spectra of TiO_2 nanotubes on the membrane (a) untreated, (b) hydrothermal and (c) vapor-thermal crystallized: [I] survey; [II] O1s region and [III] F1s region.

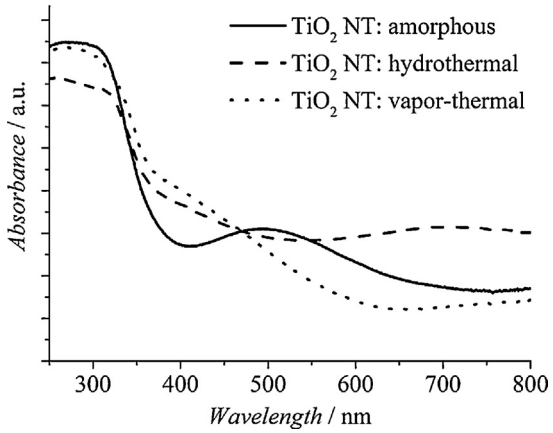

Fig. 9. UV–vis absorption spectra of amorphous and anatase TiO_2 nanotubes on the membrane. The anatase TiO_2 nanotubes were generated via hydrothermal and vapor-thermal crystallization.

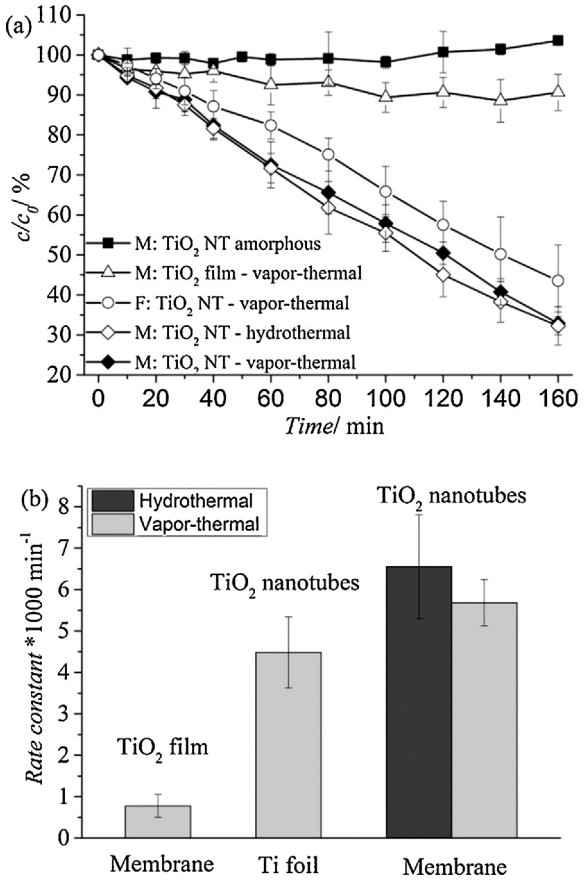

Fig. 10. Degradation of methylene blue in aqueous solution with TiO_2 nanotubes on a Ti foil (F), on top of the PES membrane (M), and a TiO_2 film on top of the PES membrane (M) crystallized via vapor-thermal treatment (110 °C, 1 h, 50 μL water) and/or hydrothermal treatment (90 °C, 2 h). (a) Degradation in percent over time, (b) rate constant of the degradation calculated via first order kinetic.

by •OH radicals which are electrostatically attracted to the TiO_2 surface to form sulfoxide group (C—S(=O)—C). The •OH radical attacks again the sulfoxide group provoking the dissociation of two benzene rings into C_6H_5-R and NH_2-C_6H_3(R)-SO_2 or SO_2-C_6H_4-R and NH_2-C_6H_4-R. The sulfone group could react under subsequent •OH attacks to sulfonic acid to form SO_4^{2-} and R-C_6H_4• radical. The R-C_6H_4• radical either reacts with •OH or H•. The N=C bonds are cleaved by •OH radicals and are mineralized to NH_4^+ and NO_3^-.

In Fig. 10a the photocatalytic activity of anatase TiO_2 nanotubes on the PES membrane and on a Ti foil are compared with the photocatalytic activity of anatase TiO_2 films on top of the PES membrane and of amorphous TiO_2 nanotubes on the PES membrane.

The amorphous TiO_2 nanotubes on the PES membrane did not degrade methylene blue; after 120 min no methylene blue removal was visible. The TiO_2 needs to be crystallized to anatase to gain photocatalytic properties [56]. A TiO_2 film on the membrane was crystallized to anatase and showed photocatalytic activity, 10% of methylene blue was eliminated after 120 min. The low photocatalytic activity of this anatase TiO_2 film is attributed to the low surface area of the TiO_2 film [25]. When synthesizing TiO_2 nanotubes on the membrane the surface area was increased and therefore the degradation of methylene blue was increased, too. After 120 min about 50% of methylene blue was eliminated and the rate constant increased from 0.8 to 5.7. The membrane as the support material led to an increase in photocatalytic activity, too. Again the gain of surface area due to porous membrane substructure compared to a flat Ti foil induced the enhanced degradation of methylene blue (Fig. 10).

The photocatalytic activity of the vapor-thermal and hydrothermal crystallized TiO_2 nanotubes on the membrane was similar. After 120 min the vapor-crystallized TiO_2 nanotubes degraded 50% and the hydrothermal crystallized TiO_2 nanotubes degraded 45% of methylene blue. Yu et al. [25] found a different behavior for vapor-thermal crystallized TiO_2 nanotubes on a Ti foil compared to hydrothermal crystallized TiO_2 nanotubes on a Ti foil. Due to the high crystallinity, large crystallite size, and the specific tubular surface area Yu et al. [25] received a higher photocatalytic activity for the vapor-thermal crystallized TiO_2 nanotubes compared to hydrothermal crystallized TiO_2 nanotubes.

In this study, the relative crystallinity and crystallite size were almost the same and could be an indication for the similar degradation behavior of differently crystallized TiO_2 nanotubes. But two different morphologies (nanoneedle and nanotubular) were obtained, which should have an impact on the rate constant due to an expected difference in surface area. Unfortunately, it was not possible to determine the difference in surface area between the two different crystalline systems by nitrogen adsorption measurements as the support material dominated the achieved values. Powder TiO_2 nanotubes crystallized via vapor-thermal treatment show a higher specific surface area than hydrothermal treated TiO_2 nanotube powders [79]. But the direct adoption of the results of the work of Yanagisawa et al. [79] are not possible due different crystallization parameters and the usage of a powder compared to a thin film here. As the relative crystallinity, the crystallite size, and the surface area are the main factors which influence the photocatalytic activity [25], and similar relative crystallinity and crystallite size values were obtained the surface area of two differently crystallized TiO_2 nanotubes should be also similar.

The crystalline phase and surface area plays a crucial role for the photocatalytic activity. While amorphous TiO_2 did not exhibit any photocatalytic activity, anatase TiO_2 showed a photocatalytic activity and when increasing the surface area due the assembly of TiO_2 and attaching it to a membrane surface the rate constant was increased enormously.

4. Conclusion

In conclusion, we demonstrated for the first time the generation of TiO_2 nanotubes on top of a porous PES polymer membrane. By using two different crystallization methods (vapor-thermal and hydrothermal), the amorphous TiO_2 was transformed to anatase TiO_2 and a nanotubular and nanoneedle-like morphology on a PES membrane was created. The relative crystallinity of the TiO_2 nanotubes obtained by vapor-thermal or hydrothermal treatment is similar and five times higher than that of calcined TiO_2 nanotubes. Furthermore, the photocatalytic activity is alike regardless of which crystallization method is used. By using the nanostructured TiO_2 to degrade methylene blue, the photocatalytic activity is increased up to 6 times compared to a TiO_2 film on the membrane. Another gain in photocatalytic activity was achieved due the usage of a porous membrane as the support material compared to a flat Ti foil. This novel design will extend the usability of the catalytic system of TiO_2 nanotubes for a stable and flexible flow through setup.

Acknowledgements

The authors are indebted to P. Hertel, A. Sobottka, A. Prager, and N. Schönherr, for magnetron sputtering of titanium to the membrane, XRD measurements, XPS measurements, and UV–vis diffuse reflectance spectroscopy measurements, respectively. Financial support by the Federal State of Germany, the Free State of Saxony and the German Federal Environmental Foundation are gratefully acknowledged.

Appendix A. Supplementary data

Supplementary data associated with this article can be found, in the online version, at http://dx.doi.org/10.1016/j.apcatb.2014.05.054.

References

[1] V. Zwilling, M. Aucouturier, E. Darque-Ceretti, Electrochim. Acta 45 (1999) 921–929.
[2] V. Zwilling, E. Darque-Ceretti, A. Boutry-Forveille, D. David, M.Y. Perrin, M. Aucouturier, Surf. Interface Anal. 27 (1999) 629–637.
[3] P. Roy, S. Berger, P. Schmuki, Angew. Chem. Int. Ed. 50 (2011) 2904–2939.
[4] X. Pan, Y. Zhao, Z. Fan, Nanosci. Nanotechnol. Lett. 4 (2012) 463–470.
[5] J. Yan, F. Zhou, J. Mater. Chem. 21 (2011) 9406–9418.
[6] Y.-Y. Kuo, C.-H. Chien, Electrochim. Acta 91 (2013) 337–343.
[7] X. Chen, C. Li, M. Gratzel, R. Kostecki, S.S. Mao, Chem. Soc. Rev. 41 (2012) 7909–7937.
[8] Z. Xu, J. Yu, Nanoscale 3 (2011) 3138–3144.
[9] L. Li, X. Liu, Y. Zhang, N.T. Nuhfer, K. Barmak, P.A. Salvador, G.S. Rohrer, ACS Appl. Mater. Interfaces 5 (2013) 5064–5071.
[10] A.W. Tan, B. Pingguan-Murphy, R. Ahmad, S.A. Akbar, Ceram. Int. 38 (2012) 4421–4435.
[11] L.M. Bjursten, L. Rasmusson, S. Oh, G.C. Smith, K.S. Brammer, S. Jin, J. Biomed. Mater. Res. A 92A (2010) 1218–1224.
[12] K. Gulati, S. Ramakrishnan, M.S. Aw, G.J. Atkins, D.M. Findlay, D. Losic, Acta Biomater. 8 (2011) 449–456.
[13] S. Minagar, C.C. Berndt, J. Wang, E. Ivanova, C. Wen, Acta Biomater. 8 (2012) 2875–2888.
[14] K. Fischer, S.G. Mayr, Adv. Mater. (Weinheim, Ger.) 23 (2011) 3838–3841.
[15] Y. Kimura, S. Kimura, R. Kojima, M. Bitoh, M. Abe, M. Niwano, Sens. Actuators B: Chem. 177 (2013) 1156–1160.
[16] D. Spitzer, T. Cottineau, N. Piazzon, S. Josset, F. Schnell, S.N. Pronkin, E.R. Savinova, V. Keller, Angew. Chem. Int. Ed. 51 (2012) 5334–5338.
[17] G. Liu, K. Wang, N. Hoivik, H. Jakobsen, Sol. Energy Mater. Sol. Cells 98 (2012) 24–38.
[18] S.P. Albu, A. Ghicov, J.M. Macak, R. Hahn, P. Schmuki, Nano Lett. 7 (2007) 1286–1289.
[19] J. Kim, J. Cho, J. Electrochem. Soc. 154 (2007) A542–A546.
[20] G.F. Ortiz, I. Hanzu, P. Knauth, P. Lavela, J.L. Tirado, T. Djenizian, Electrochim. Acta 54 (2009) 4262–4268.
[21] S.K. Mohapatra, V.K. Mahajan, M. Misra, Nanotechnology 18 (2007) 445705.
[22] B. Liu, K. Nakata, S. Liu, M. Sakai, T. Ochiai, T. Murakami, K. Takagi, A. Fujishima, J. Phys. Chem. C 116 (2012) 7471–7479.
[23] X. Zhang, J.H. Pan, W. Fu, A.J. Du, D.D. Sun, Water Sci. Technol.: Water Supply 9 (2009) 45–49.
[24] Y.-K. Lai, J.-Y. Huang, H.-F. Zhang, V.-P. Subramaniam, Y.-X. Tang, D.-G. Gong, L. Sundar, L. Sun, Z. Chen, C.-J. Lin, J. Hazard. Mater. 184 (2010) 855–863.
[25] J. Yu, G. Dai, B. Cheng, J. Phys. Chem. C 114 (2010) 19378–19385.
[26] J. Yu, G. Wang, B. Cheng, M. Zhou, Appl. Catal. B: Environ. 69 (2007) 171–180.
[27] J.C. Yu, J. Yu, W. Ho, Z. Jiang, L. Zhang, Chem. Mater. 14 (2002) 3808–3816.
[28] J. Xu, Y. Ao, M. Chen, D. Fu, Appl. Surf. Sci. 256 (2010) 4397–4401.
[29] I. Paramasivam, H. Jha, N. Liu, P. Schmuki, Small 8 (2012) 3073–3103.
[30] C.A. Grimes, G.K. Mor, TiO_2 Nanotube Arrays, Springer, Dordrecht, 2009.
[31] Q. Cai, M. Paulose, O.K. Varghese, C.A. Grimes, J. Mater. Res. 20 (2005) 230–236.
[32] Y. Tang, J. Tao, Z. Dong, J.T. Oh, Z. Chen, Adv. Nat. Sci.: Nanosci. Nanotechnol. 2 (2011) 045002.
[33] N.K. Allam, C.A. Grimes, Sol. Energy Mater. Sol. Cells 92 (2008) 1468–1475.
[34] S. Yoriya, G.K. Mor, S. Sharma, C.A. Grimes, J. Mater. Chem. 18 (2008) 3332–3336.
[35] S. Yoriya, M. Paulose, O.K. Varghese, G.K. Mor, C.A. Grimes, J. Phys. Chem. C 111 (2007) 13770–13776.
[36] K. Shankar, G.K. Mor, A. Fitzgerald, C.A. Grimes, J. Phys. Chem. C 111 (2006) 21–26.
[37] M. Paulose, H.E. Prakasam, O.K. Varghese, L. Peng, K.C. Popat, G.K. Mor, T.A. Desai, C.A. Grimes, J. Phys. Chem. C 111 (2007) 14992–14997.
[38] N.K. Allam, K. Shankar, C.A. Grimes, J. Mater. Chem. 18 (2008) 2341–2348.
[39] A. Chaudhary, T.H. Choudhury, S. Naik, S. Raghavan, J. Am. Ceram. Soc. 95 (2012) 64–66.
[40] V. Galstyan, A. Vomiero, E. Comini, G. Faglia, G. Sberveglieri, RSC Adv. 1 (2011) 1038–1044.
[41] V. Galstyan, A. Vomiero, I. Concina, A. Braga, M. Brisotto, E. Bontempi, G. Faglia, G. Sberveglieri, Small 7 (2011) 2437–2442.
[42] C.G. Kuo, C.Y. Hsu, S.S. Wang, D.C. Wen, Appl. Surf. Sci. 258 (2012) 6952–6957.
[43] S.L. Lim, Y. Liu, J. Li, E.-T. Kang, C.K. Ong, Appl. Surf. Sci. 257 (2011) 6612–6617.
[44] J.M. Macak, H. Tsuchiya, S. Berger, S. Bauer, S. Fujimoto, P. Schmuki, Chem. Phys. Lett. 428 (2006) 421–425.
[45] H. Nanjo, F.M.B. Hassan, S. Venkatachalam, N. Teshima, K. Kawasaki, T. Aizawa, T. Aida, T. Ebina, J. Power Sources 195 (2010) 5902–5908.
[46] J. Ni, C.J. Frandsen, K. Noh, G.W. Johnston, G. He, T. Tang, S. Jin, Mater. Sci. Eng. C 33 (2013) 1460–1466.
[47] Y.-X. Tang, J. Tao, Y.-Y. Zhang, T. Wu, H.-J. Tao, Y.-R. Zhu, Trans. Nonferr. Metals Soc. China 19 (2009) 192–198.
[48] O.K. Varghese, M. Paulose, C.A. Grimes, Nat. Nano 4 (2009) 592–597.

[49] A. Vomiero, V. Galstyan, A. Braga, I. Concina, M. Brisotto, E. Bontempi, G. Sberveglieri, Energy Environ. Sci. 4 (2011) 3408–3413.
[50] J. Weickert, C. Palumbiny, M. Nedelcu, T. Bein, L. Schmidt-Mende, Chem. Mater. 23 (2011) 155–162.
[51] Q. Chen, D. Xu, J. Phys. Chem. C 113 (2009) 6310–6314.
[52] D. Wang, Y. Liu, C. Wang, F. Zhou, W. Liu, ACS Nano 3 (2009) 1249–1257.
[53] M.M. Byranvand, K. Ali Nemati, B. Mohammad Hossein, Nano-Micro Lett. 4 (2012) 253–266.
[54] W. Krengvirat, S. Sreekantan, A.-F. Mohd Noor, N. Negishi, G. Kawamura, H. Muto, A. Matsuda, Mater. Chem. Phys. 137 (2013) 991–998.
[55] W. Zhu, X. Liu, H. Liu, D. Tong, J. Yang, J. Peng, Electrochim. Acta 56 (2011) 2618–2626.
[56] J. Yu, B. Wang, Appl. Catal. B: Environ. 94 (2010) 295–302.
[57] A.H. Yuwono, N. Sofyan, I. Kartini, A. Ferdiansyah, T.H. Pujianto, Adv. Mater. Res. 277 (2011) 90–99.
[58] A. Houas, H. Lachheb, M. Ksibi, E. Elaloui, C. Guillard, J.-M. Herrmann, Appl. Catal. B: Environ. 31 (2001) 145–157.
[59] Q. Zhang, H. Xu, W. Yan, Nanosci. Nanotechnol. Lett. 4 (2012) 505–519.
[60] Y.W. Yan Wang, G. Xu, Y. Qin, H. Zheng, J. Cui, Y. Hong, L. Liu, X. Shu, Y. Zheng, X. Huang, J. Appl. Electrochem. 42 (2012) 1013–1024.
[61] D. Wang, Y. Liu, B. Yu, F. Zhou, W. Liu, Chem. Mater. 21 (2009) 1198–1206.
[62] D.K. Platt, Engineering and High Performance Plastics – Market Report, Rapra Technology Limited, 2003.
[63] D. Wang, L. Liu, F. Zhang, K. Tao, E. Pippel, K. Domen, Nano Lett. 11 (2011) 3649–3655.
[64] Y. Liao, W. Que, P. Zhong, J. Zhang, Y. He, ACS Appl. Mater. Interfaces 3 (2011) 2800–2804.
[65] A.H. Yuwono, N. Sofyan, I. Kartini, A. Ferdiansyah, T.H. Pujianto, Adv. Mater. Res. 277 (2011) 90.
[66] C. Su, L. Liu, M. Zhang, Y. Zhang, C. Shao, CrystEngComm 14 (2012) 3989–3999.
[67] M. Kanna, S. Wongnawa, S. Buddee, K. Dilokkhunakul, P. Pinpithak, J. Sol–Gel Sci. Technol. 53 (2010) 162–170.
[68] B. Prasai, B. Cai, M.K. Underwood, J. Lewis, D.A. Drabold, J. Mater. Sci. 47 (2012) 7515–7521.
[69] J.M. Peralta-Hernández, J. Manríquez, Y. Meas-Vong, F.J. Rodríguez, T.W. Chapman, M.I. Maldonado, L.A. Godínez, J. Hazard. Mater. 147 (2007) 588–593.
[70] D.M. Blake, Bibliography of Work on the Heterogeneous Photocatalytic Removal of Hazardous Compounds from Water and Air, National Renewable Energy Laboratory, 2001.
[71] P. Calza, V.A. Sakkas, C. Medana, C. Baiocchi, A. Dimou, E. Pelizzetti, T. Albanis, Appl. Catal. B: Environ. 67 (2006) 197–205.
[72] O.K. Dalrymple, D.H. Yeh, M.A. Trotz, J. Chem. Technol. Biotechnol. 82 (2007) 121–134.
[73] U.I. Gaya, A.H. Abdullah, J. Photochem. Photobiol. C: Photochem. Rev. 9 (2008) 1–12.
[74] N. Miranda-García, M.I. Maldonado, J.M. Coronado, S. Malato, Catal. Today 151 (2010) 107–113.
[75] X.-D. Zhu, Y.-J. Wang, R.-J. Sun, D.-M. Zhou, Chemosphere 92 (2013) 925–932.
[76] A.S. Giri, A.K. Golder, Ind. Eng. Chem. Res. 53 (2014) 1351–1358.
[77] M. Antonopoulou, I. Konstantinou, Catal. Today (2014), http://dx.doi.org/10.1016/j.cattod.2014.03.027, in press.
[78] Q. Xiang, J. Yu, P.K. Wong, J. Colloid Interface Sci. 357 (2011) 163–167.
[79] K. Yanagisawa, J. Ovenstone, J. Phys. Chem. B 103 (1999) 7781–7787.